Available online at www.sciencedirect.com
SCIENCE DIRECT
Journal of Catalysis 229 (2005) 72–81
JOURNAL OF CATALYSIS
www.elsevier.com/locate/jcat

Thermolytic conversion of a bis(alkoxy)tris(siloxy)tantalum(V) single-source molecular precursor to catalytic tantala–silica materials

Richard L. Brutchey, Claus G. Lugmair, Lars O. Schebaum, T. Don Tilley *

Department of Chemistry, University of California, Berkeley, CA 94720-1460, USA
Chemical Sciences Division, Lawrence Berkeley National Laboratory, 1 Cyclotron Road, Berkeley, CA 94720, USA

Received 1 September 2004; revised 13 October 2004; accepted 19 October 2004

Available online 24 November 2004

Abstract

The new complex $(^{i}PrO)_2Ta[OSi(O^{t}Bu)_3]_3$ (**1**) was prepared via silanolysis of $Ta(O^{i}Pr)_5$ with $(^{t}BuO)_3SiOH$ and is a useful structural and spectroscopic (NMR, FTIR) model of Ta(V) on silica. The complex was also used to prepare tantalum-containing silica materials, via the thermolytic molecular precursor method (yielding $Ta_2O_5 \cdot 6SiO_2$ and $Ta_2O_5 \cdot 18SiO_2$) or by grafting **1** onto mesoporous SBA-15 silica (yielding a surface-supported tantala species, TaSBA-15). The solution phase thermolysis of **1** in nonpolar media afforded homogeneous, high-surface-area (ca. 450 $m^2\,g^{-1}$) xerogels ($Ta_2O_5 \cdot 6SiO_2$) that are amorphous up to approximately 1100 °C. A more silica-rich tantala–silica material ($Ta_2O_5 \cdot 18SiO_2$) was prepared via a solution-phase co-thermolytic route with 1 and $HOSi(O^{t}Bu)_3$, to yield a material with a Si/Ta ratio of 9/1. It was demonstrated that tantala–silica materials are active as catalysts for cyclohexene oxidation.

Keywords: Tantalum; Silicon; Molecular precursor route; Amorphous materials; Supported catalysts; Oxidation; Peroxides

1. Introduction

The rational design and development of new catalytic materials, for which the arrangements of atoms and nanostructures are well defined, remains a formidable challenge for chemists and materials scientists [1–3]. One method that has received considerable attention is the low-temperature sol–gel route, which can produce metal oxide materials through the hydrolysis and condensation of metal alkoxide precursors (typically in polar media) [4–6]. One drawback to this method is that the formation of homogeneous, mixed metal oxide materials is complicated by the inherently different hydrolysis rates for the various metal alkoxide precursors. Thus it is often difficult to optimize the homogeneity of the resultant materials, especially without special precautions and optimized experimental conditions [4–13].

One alternative to the sol–gel method relies on the use of single-source molecular precursors [14–22]. Such precursors possess a defined ratio of elements to be incorporated into the target material and provide a low-temperature, kinetically controlled pathway to homogeneous, mixed metal oxide materials. A number of such precursors, which are transition metal tris(*tert*-butoxy)siloxy complexes of the type $M[OSi(O^{t}Bu)_3]_n$, have been prepared and studied [23–27]. These oxygen-rich molecular precursors can be thermolytically converted to amorphous, homogeneous transition metal oxide–silica materials. Upon heating (usually below 200 °C), these molecular precursors eliminate isobutylene and water to give the transition metal oxide–silica material, either in the solid state or in nonpolar media. Solution thermolyses of the molecular precursors afford high-surface-area xerogels upon air-drying.

Silica-supported group V materials are known to be potentially interesting alkene oxidation catalysts [28–35]. Although considerable attention has been devoted to vanadium and niobium silica-supported catalysts, only a few studies have addressed the synthesis of silica-supported tanta-

* Corresponding author.
E-mail address: tdtilley@socrates.berkeley.edu (T.D. Tilley).

0021-9517/$ – see front matter
doi:10.1016/j.jcat.2004.10.015

lum alkene oxidation catalysts [29,30]. Here we report the synthesis and characterization of a single-source molecular precursor, $(^{i}PrO)_2Ta[OSi(O^{t}Bu)_3]_3$ (**1**), and its thermolytic conversion to tantala–silica materials. These materials have been studied as cyclohexene oxidation catalysts.

2. Experimental

2.1. General procedures

All manipulations were conducted under a nitrogen atmosphere with the use of standard Schlenk techniques, or in a Vacuum Atmospheres drybox, unless otherwise noted. Dry, oxygen-free solvents were used throughout. Benzene-d_6 was purified and dried by vacuum distillation from sodium/potassium alloy.

$TaCl_5$ was purchased from Strem Chemicals, Inc., and sublimed prior to use. *iso*-Propyl alcohol and triethylamine were purchased from Aldrich and distilled from calcium hydride prior to use. Cyclohexene was purchased from Aldrich and distilled prior to use. Aqueous hydrogen peroxide (H_2O_2) (30%), cumene hydroperoxide (CHP) (80%), and *tert*-butyl hydroperoxide (TBHP) (5.5 M in decane) were purchased from Aldrich and used as received. $Ta(O^{i}Pr)_5$ [36], $(^{t}BuO)_3SiOH$ [37], and SBA-15 [38] were prepared as reported in the literature.

2.2. Synthesis of $(^{i}PrO)_2Ta[OSi(O^{t}Bu)_3]_3$ (1)

A pentane (20 ml) solution of $(^{t}BuO)_3SiOH$ (8.43 mmol) was added to a pentane (10 ml) solution of $Ta(O^{i}Pr)_5$ (1.67 mmol) in a Schlenk tube under flowing nitrogen at 0 °C. The reaction mixture was warmed to room temperature, and stirring was continued for 15 h. Subsequent removal of the volatile materials in vacuo (25 °C) yielded a white solid, at which point excess $(^{t}BuO)_3SiOH$ was sublimed away from the product (70 °C, 0.001 mm Hg, 4 h). The white solid was taken up in a pentane/toluene (ca. 1/1, vol/vol) solvent mixture and kept at −78 °C for 72 h. Analytically pure colorless crystals were isolated at −78 °C (93%). (Anal. Calcd. for $C_{42}H_{95}Si_3O_{14}Ta$ (%): C, 46.31; H, 8.97. Found: C, 46.37; H, 8.59. FTIR (cm^{-1}): 1389 w, 1365 m, 1242 m, 1192 m, 1114 m, 1071 s, 944 s, 831 w, 802 vw, 701 m, 651 vw, 568 w, 550 w sh, 514 vw, 490 w sh, 469 m, 457 w sh, 433 w. ^1H NMR (benzene-d_6, 25 °C, 400 MHz): δ 5.49 (sept, 2 H, $J = 6.1$ Hz, $Ta(O^{i}Pr)$), 1.52 (s, 81 H, $Si(O^{t}Bu)$), 1.46 (d, 12 H, $J = 6.1$ Hz, $Ta(O^{i}Pr)$). $^{13}C\{^1H\}$ NMR (benzene-d_6, 25 °C, 100 MHz): δ 75.28 $Ta(O^{i}Pr)$, 72.91 $Si(O^{t}Bu)$, 31.87 $Si(O^{t}Bu)$, 26.96 $Ta(O^{i}Pr)$. $^{29}Si\{^1H\}$ NMR (benzene-d_6, 25 °C, 99.4 MHz): δ −97.57.)

2.3. Gelation of 1 in toluene [$Ta_2O_5 \cdot 6SiO_2$]

A toluene solution of **1** (0.361 g, 0.06 M) was sealed in a 20-ml Parr reactor in a drybox under a nitrogen atmosphere. The reactor was placed in a preheated oven (180 °C) for 24 h. The wet gel was removed and air-dried for 1 week to form a xerogel. The xerogel was rinsed with pentane (2 × 5 ml) and toluene (2 × 5 ml) and was allowed to air-dry for 1 day. The off-white xerogel was ground into a fine powder and dried in vacuo for 12 h at 120 °C to yield 0.110 g of material. Repeated syntheses of $Ta_2O_5 \cdot 6SiO_2$ yielded materials with similar carbon and hydrogen contents, and the same surface areas (within experimental error).

2.4. Gelation of 1 and $(^{t}BuO)_3SiOH$ in toluene [$Ta_2O_5 \cdot 18SiO_2$]

A 6.0-ml toluene solution of **1** (0.462 mol) and $(^{t}BuO)_3SiOH$ (2.760 mol) was sealed in a 20-ml Parr reactor in a drybox under a nitrogen atmosphere. The reactor was placed in a preheated oven (180 °C) for 24 h. The wet gel was removed and air-dried for 7 days to form a xerogel. The xerogel was rinsed with hexanes (2 × 5 ml) and toluene (2 × 5 ml) and was allowed to air-dry for 1 day. The off-white xerogel was ground into a fine powder and dried in vacuo for 12 h at 120 °C to yield 0.323 g of material.

2.5. Preparation of TaSBA-15

The SBA-15 was dried at 130 °C in vacuo for 15 h and handled under a nitrogen atmosphere thereafter. A 0.121-g sample of SBA-15 was suspended in pentane (25 ml). A pentane solution (30 ml) of **1** (0.016 g) was prepared and then added to the stirred suspension of SBA-15 (25 °C). The resulting mixture was stirred for 15 h and then filtered and washed with pentane (3 × 20 ml). The grafted material was dried for 2–3 h in vacuo to yield the as-prepared catalyst with 1.51 wt% tantalum loading (TaSBA-15, SA = 310 $m^2\,g^{-1}$), as determined by inductively coupled atomic emission spectroscopy (ICPAES). A subsequent catalyst was prepared by calcination of this material to 300 °C (10 °C min^{-1}) under a flow of oxygen for 4 h.

2.6. Catalysis procedure

A sample of catalyst (0.035 g) was added to a 50-ml round-bottom flask that was fitted with a reflux condenser and a septum. Acetonitrile (5.0 ml) and cyclohexene (2.5 ml) were added by syringe through the septum under a flow of nitrogen. Dodecane (50.0 µl) or toluene (23 µl) was added as an internal standard. The mixture was allowed to equilibrate at the reaction temperature of 65 °C for 10 min. Aqueous H_2O_2 (0.62 ml), CHP (1.0 ml), or TBHP (1.0 ml) was added by syringe to the rapidly stirred solution. Aliquots (ca. 0.08 ml) were removed from the reaction mixture by syringe after 5, 30, 60, 90, and 120 min and then filtered and

cooled. The filtrate was analyzed by gas chromatography (GC), and assignments were made by comparison with authentic samples analyzed under the same conditions.

2.7. Characterization

Solution ^{1}H NMR spectra were recorded at 400 MHz with a Bruker AM-400 spectrometer and were referenced internally to the residual solvent proton signal relative to tetramethylsilane. Similarly, solution ^{13}C and ^{29}Si NMR spectra were recorded at 100 and 99.4 MHz, respectively. ^{29}Si MAS NMR data were collected on a CMX400 Infinity spectrometer based on a 9.4-T magnet, with a frequency of 79.4867 MHz, a spectrum width of 50 kHz, a 90° pulse length of 4 μs, and a pulse delay of 30 s. A direct polarization pulse sequence was used with a 3-μs pulse length. Tetramethylsilane was used as an external chemical shift reference, and samples were spun at 7–10 kHz. Infrared spectra were recorded as KBr disks with a Mattson FTIR spectrometer. Elemental analyses were performed at the College of Chemistry microanalytical laboratory at the University of California, Berkeley, and Galbraith Laboratories, Inc. PXRD experiments were performed on a Siemens D5000 X-ray diffractometer with the use of Cu-K_α radiation. Transmission electron microscopy was carried out on a Topcon EM-002B transmission electron microscope operating at 200 kV. Samples for energy-dispersive spectroscopy (EDS) were studied on a JEOL JEM-200CX transmission electron microscope operating at 160 kV. EDS spectra were taken on a Gatan detector connected to the electron microscope, and atomic compositions were quantified with the use of the Si-*K* and Ta-*L* lines. We prepared samples for TEM studies by depositing a pentane suspension of the finely ground xerogels on carbon-coated copper or gold grids obtained from Ted Pella, Inc. Nitrogen adsorption isotherms were performed on a Quantachrome Autosorb 1 surface area analyzer, and samples were outgassed at 120 °C for at least 15 h prior to measurement. Thermal analyses were performed on a TA Instruments SDT 2960 Integrated TGA/DSC analyzer at a heating rate of 10 °C min^{-1} under a flow of nitrogen or oxygen. Calcinations were performed with the use of a Lindberg 1200 °C three-zone furnace at a heating rate of 10 °C min^{-1} under a flow of oxygen, and the temperature was held constant for 4 h. GC analyses were performed with an HP 6890 GC system and a methyl siloxane capillary (50.0 m × 320 μm × 1.05 μm nominal), and integration was performed relative to dodecane or toluene.

2.8. Structural determination for **2**

Crystals of **2** were grown from a concentrated pentane solution at −40 °C. A colorless blocky crystal with dimensions of 0.36 × 0.30 × 0.25 mm was mounted on a glass fiber with Paratone N hydrocarbon oil. Data were collected with a Siemens SMART diffractometer with a CCD area detector. We determined a preliminary orientation matrix and unit cell parameters by collecting 60 10-s frames, followed by spot integration and least-squares refinement. A hemisphere of data was collected with ω scans of 0.3° and a collection time of 10 s per frame. Frame data were integrated (XY spot spread = 1.60°; Z spot spread = 0.60°) with the use of SAINT. The data were corrected for Lorentz and polarization effects. An absorption correction was performed with XPREP ($\mu R = 0.2$, $T_{max} = 0.62$, $T_{min} = 0.50$). The 22,872 integrated reflections were averaged in point group 2/m to give 8238 unique reflections ($R_{int} = 0.050$). Of these, 4953 reflections were considered to be observed ($I > 3.00\sigma(I)$). No decay correction was necessary. Inspection of the systematic absences uniquely defined the space group $P2_1/n$. The structure was solved with direct methods (SIR92) and refined by full matrix least-squares methods with teXsan software. Four oxygen atoms that were modeled as disordered over two sites [O(9)–O(10), O(11)–O(12), O(15)–O(16), O(17)–O(18)] were refined isotropically. The remaining non-hydrogen atoms were refined anisotropically. The hydrogen atoms were included at calculated positions but not refined. The number of variable parameters was 519, giving a data/parameter ratio of 9.54. The maximum and minimum peaks on the final difference Fourier map corresponded to 1.85 and −1.70 e/Å^3: $R = 0.044$, $R_w = 0.064$, GOF = 2.11.

3. Results and discussion

3.1. Synthesis and characterization of (^{i}PrO)$_2$Ta[OSi(O^{t}Bu)$_3$]$_3$ (**1**)

The tantalum complex (**1**) was prepared by the addition of a pentane solution of (^{t}BuO)$_3$SiOH (5 equiv) to a pentane solution of Ta(O^{i}Pr)$_5$

$$\mathrm{Ta(O^{\,i}Pr)_5} + 5\mathrm{HOSi(O^{\,t}Bu)_3} \xrightarrow[-3\mathrm{HO^{\,i}Pr}]{\text{pentane}} (^i\mathrm{PrO})_2\mathrm{Ta[OSi(O^{\,t}Bu)_3]_3}. \quad (1)$$

The product, (^{i}PrO)$_2$Ta[OSi(O^{t}Bu)$_3$]$_3$ (**1**), was crystallized from a pentane/toluene mixture (50/50, vol/vol) at −78 °C to yield analytically pure, colorless crystals. For comparison, Wolczanki has reported tantalum complexes containing no more than three silox (^{t}Bu$_3$SiO–) ligands [39]. In contrast, Bradley has reported the homoleptic siloxide Ta(OSiMe$_3$)$_5$ as containing the less sterically demanding –OSiMe$_3$ ligand [40].

Crystals of sufficient quality to acquire a single-crystal X-ray structure of **1** could not be obtained, but an analogous precursor, (EtO)$_2$Ta[OSi(O^{t}Bu)$_3$]$_3$ (**2**), was synthesized in a similar fashion. The structure of **2** was unequivocally determined by single-crystal X-ray structure analysis.[1] The

[1] Crystallographic data for **2**. Crystal dimensions (mm): 0.36 × 0.30 × 0.25. Crystal system: monoclinic. Space group: $P2_1/n$. Unit cell dimensions and volume: $a = 13.7006(2)$ Å, $b = 16.9122(1)$ Å, $c = 24.1526(4)$ Å,

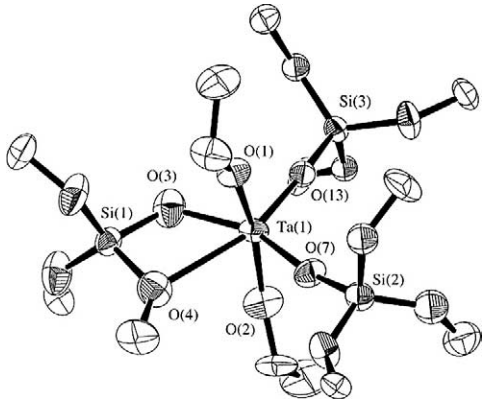

Fig. 1. ORTEP diagram of $(EtO)_2Ta[OSi(O^tBu)_3]_3$ (**2**) at the 50% probability level. Terminal methyl groups (on the ^tBuO– groups) and hydrogen atoms have been omitted for clarity.

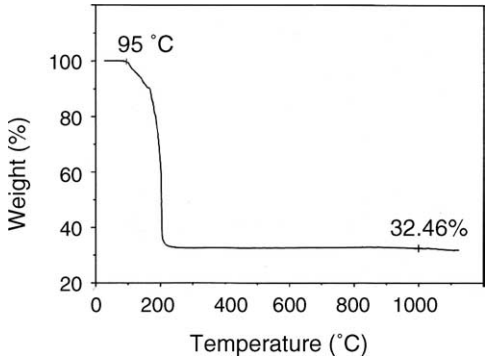

Fig. 2. TGA trace for **1** under a flow of nitrogen, with a heating rate of 10 °C min^{-1}.

ORTEP diagram of **2** is shown in Fig. 1, and bond distances and angles are reported in the Supplementary Information. In complex **2** the five covalently bound ligands, in addition to one datively bound O^tBu group, form an approximately octahedral coordination environment about the tantalum metal center. This type of bonding mode for a datively bound O^tBu group from the $–OSi(O^tBu)_3$ ligand has been observed previously in the solid-state structures of $Zr[OSi(O^tBu)_3]_4$ and $Hf[OSi(O^tBu)_3]_4$ [41]. The Ta–OSi bond distances ranged from 1.860(5) to 2.041(7) Å and are similar to the Ta–OSi bond distances (1.80–1.94 Å) previously determined for silica-supported tantalum by EXAFS analysis [42].

3.2. Thermolytic conversion of *1* to $Ta_2O_5 \cdot 6SiO_2$

The decomposition behavior of **1** was studied by thermogravimetric analysis (TGA). The TGA trace for **1** (Fig. 2) shows an onset for weight loss at ca. 95 °C with a precipitous weight loss occurring at ca. 200 °C (under flowing nitrogen, heated at 10 °C min^{-1}). After heating to 1000 °C, a ceramic yield of 32.5% was obtained, which is 4.3% lower than the expected ceramic yield for stoichiometric formation of $Ta_2O_5 \cdot 6SiO_2$ (36.8% expected). Analysis of the volatile by-products (by ^{1}H NMR spectroscopy), trapped from the solid-state decomposition of **1** by vacuum transfer, revealed a significant quantity of $(^tBuO)_3SiOH$ (0.32 equiv) in addition to isobutylene. The volatilization of silanol is responsible for the slightly reduced ceramic yields observed by TGA. The solubility of **1** in organic solvents makes it possible to carry out the thermal decomposition in solution. The decomposition of **1** was monitored by solution ^{1}H NMR spectroscopy and the quantification of the soluble decomposition products against an internal standard (ferrocene) in benzene-d_6. Heating at 160 °C for 24 h resulted in the complete conversion of **1**; the major products observed were isobutylene (7.5 equiv) and isopropanol (1.3 equiv). Gel formation was observed within 2 h.

Bulk samples of $Ta_2O_5 \cdot 6SiO_2$ were obtained via solution-phase thermolyses (150–180 °C) of **1** in isooctane or toluene (ca. 0.06 M) in a sealed Parr reactor under an atmosphere of nitrogen for 24 h. This produced white gels that occupied the entire volume of the original solution. Upon air-drying for several days, the gels shrank to ca. 30% of their original volume and became hard, white materials. The gels were washed with pentane and toluene and then air-dried again overnight. The final xerogels were then ground into a fine powder and dried in vacuo (120 °C) for 12 h to provide the as-prepared $Ta_2O_5 \cdot 6SiO_2$ material.

3.3. Co-thermolytic synthesis of $Ta_2O_5 \cdot 18SiO_2$

Previously we reported the co-thermolysis of a zirconium-containing molecular precursor with $Si(OEt)_4$ (TEOS) to produce homogeneous zirconia–silica materials with tunable silicon to zirconium ratios [27]. Similarly, co-thermolyses of the tantalum-containing molecular precursor (**1**) with $(^tBuO)_3SiOH$ readily yielded tantala–silica materials. Notably, the silanol ligand does not thermally convert to silica in the absence of tantalum. Solution ^{1}H NMR spectroscopic studies demonstrated that heating benzene-d_6 solutions of **1** and $(^tBuO)_3SiOH$ (1:5.2 mol ratios) to 160 °C resulted in gel formation within 2 h. The precursors $(^tBuO)_3SiOH$ and **1** were completely consumed and incorporated into the material after 2 h, and isobutylene (25 equiv) was quantitatively observed as the only decomposition product. Increasing the molar ratio of **1** to $(^tBuO)_3SiOH$ beyond 1/6 resulted in incomplete thermal decomposition of $(^tBuO)_3SiOH$ after heating at 160 °C for 24 h.

Bulk samples of $Ta_2O_5 \cdot 18SiO_2$ were prepared by combining **1** and $(^tBuO)_3SiOH$ (1/6 mol ratio) in a toluene solution and heating in a Parr reactor under nitrogen at 180 °C for 24 h. This preparation yielded a monolithic, white gel that was air-dried for 1 week, washed with hexanes and toluene, and then air-dried again for 1 day. The final xerogel was then

$\beta = 93.049(1)°$, $V = 5588.1(1)$ Å^3. $\rho_{calc} = 1.261$ g cm^{-3}. Radiation: Mo-K$_\alpha$ ($\lambda = 0.71069$ Å). Scan type: ω (0.3 degrees per frame). Temperature of measurement: −110 °C. No. of reflections measured: total = 22,872, unique = 8238. $R_{obs} = 0.044$, $wR2_{obs} = 0.064$, $GOF_{obs} = 2.11$.

ground into a fine powder and dried in vacuo at 120 °C for 12 h.

3.4. Characterization of tantala–silica materials

By elemental analysis (inductively coupled plasma atomic emission spectroscopy), the Si/Ta ratio for $Ta_2O_5 \cdot 6SiO_2$ was found to be 2.88/1, which is very close to the expected ratio of 3/1. The elemental composition and homogeneity for $Ta_2O_5 \cdot 18SiO_2$ were probed by energy-dispersive X-ray spectroscopy (EDS). EDS profiles taken from local portions (ca. 30 nm) of the $Ta_2O_5 \cdot 18SiO_2$ xerogel revealed a Si/Ta ratio of 8.34/1, which is within 10% of the expected value and constant over randomly sampled local areas. The carbon content for $Ta_2O_5 \cdot 6SiO_2$ was found to be quite low (0.72%) by combustion analysis. After calcination to 500 °C under flowing oxygen, the carbon content remained unchanged (0.75%). The carbon content for $Ta_2O_5 \cdot 18SiO_2$ was found to be 2.61% by combustion analysis and 0.25% after calcination to 500 °C under flowing oxygen. Carbon in the uncalcined, silica-rich $Ta_2O_5 \cdot 18SiO_2$ xerogel most likely comes from *tert*-butyl groups from $HOSi(O^tBu)_3$ added to the thermolysis mixture and is not uncommon for the thermolytic molecular precursor route [27]. Thermogravimetric analysis of $Ta_2O_5 \cdot 6SiO_2$ with a heating rate of 10 °C min^{-1} under oxygen revealed a mass loss of 3.4% up to 350 °C, which probably corresponds to physisorbed and chemisorbed water and organic species [43]. Likewise for $Ta_2O_5 \cdot 18SiO_2$, TGA revealed a mass loss of 4.6% when heated to 350 °C. Heating these materials to 1000 °C resulted in an additional 1.0–3.0 wt% loss.

The crystallization behavior of $Ta_2O_5 \cdot 6SiO_2$ as a function of temperature was studied by powder X-ray diffraction (PXRD). The xerogel derived from **1** remained amorphous up to 1100 °C, when domains of the orthorhombic, low-temperature form of Ta_2O_5 (L-Ta_2O_5) were detected [44]. Upon further calcination to 1300 °C the peaks in the PXRD spectrum sharpened with increasing crystallite size. The xerogel derived from the co-thermolysis of **1** and $HOSi(O^tBu)_3$ remained amorphous until the temperature went above 1000 °C, where domains of L-Ta_2O_5 were first detected by very broad features in the PXRD pattern. As with other multicomponent mixed-oxide ceramics, the temperature at which a single-component phase segregates and crystallizes can be used as a gauge of the original homogeneity of the mixed-oxide material. For homogeneous mixed oxides, more extensive diffusion must occur prior to nucleation and grain growth of the crystalline phase [43,45,46]. This will delay the appearance of crystalline single-component oxides. Bulk Ta_2O_5 crystallizes into L-Ta_2O_5 at ca. 750 °C, whereas $Ta_2O_5 \cdot 6SiO_2$ and $Ta_2O_5 \cdot 18SiO_2$ required calcination to a temperature above 1000 °C before L-Ta_2O_5 was observed. Similarly, Guiu and Grange found that a sol–gel-derived $Ta_2O_5 \cdot 5.2SiO_2$ mixed oxide required calcination to 1200 °C before crystalline L-Ta_2O_5 was observed [43].

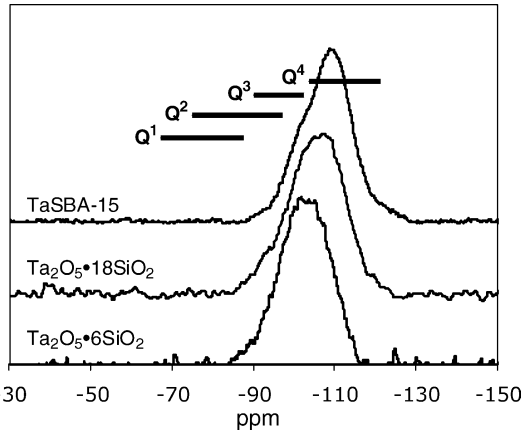

Fig. 3. ^{29}Si MAS NMR spectra of $Ta_2O_5 \cdot 6SiO_2$, $Ta_2O_5 \cdot 18SiO_2$, and TaSBA-15 showing Q^1, Q^2, Q^3, and Q^4 ranges of chemical shifts from inorganic framework silicon atoms.

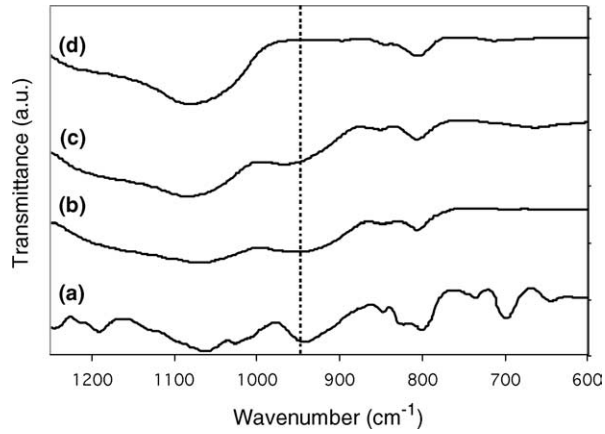

Fig. 4. Room temperature FTIR spectra of **1** (a), $Ta_2O_5 \cdot 6SiO_2$ (b), $Ta_2O_5 \cdot 18SiO_2$ (c), and TaSBA-15 (d). The Ta–O–Si asymmetric stretching band is highlighted with a dashed line.

The molecular precursor **1** can serve as a spectroscopic model for tantala–silica materials. The observed ^{29}Si NMR resonance for **1** at −97.57 ppm is in the region expected for M–$OSi(O^tBu)_3$ sites. The silicon environments of $Ta_2O_5 \cdot 6SiO_2$ and $Ta_2O_5 \cdot 18SiO_2$ were examined by solid-state ^{29}Si MAS NMR spectroscopy with the use of direct polarization and are typical of amorphous silica networks (Fig. 3). The ^{29}Si MAS NMR spectra reveal broad resonances centered at −103 ppm for $Ta_2O_5 \cdot 6SiO_2$ and −108 ppm for $Ta_2O_5 \cdot 18SiO_2$ that span the chemical shift range for Q^2, Q^3, and Q^4 silicon environments. The ^{29}Si NMR spectrum for $Ta_2O_5 \cdot 18SiO_2$ is shifted toward the Q^4 ($Si–(OSi)_4$) chemical shift range, as expected for the more silicon-rich xerogel. The FTIR spectrum of **1** exhibits strong Si–O–Si and Si–O–C overlapping bands centered at 1065 cm^{-1} (Fig. 4). A strong band centered at 944 cm^{-1} is observed for the Ta–O–Si asymmetric stretching mode [47,48]. The FTIR spectra of both $Ta_2O_5 \cdot 6SiO_2$ and $Ta_2O_5 \cdot 18SiO_2$ display a strong band for Si–O–Si at 1085 and 1078 cm^{-1}, respectively. Both materials exhibit the characteristic band at 951 and 969 cm^{-1}, respectively, for the Ta–O–Si asym-

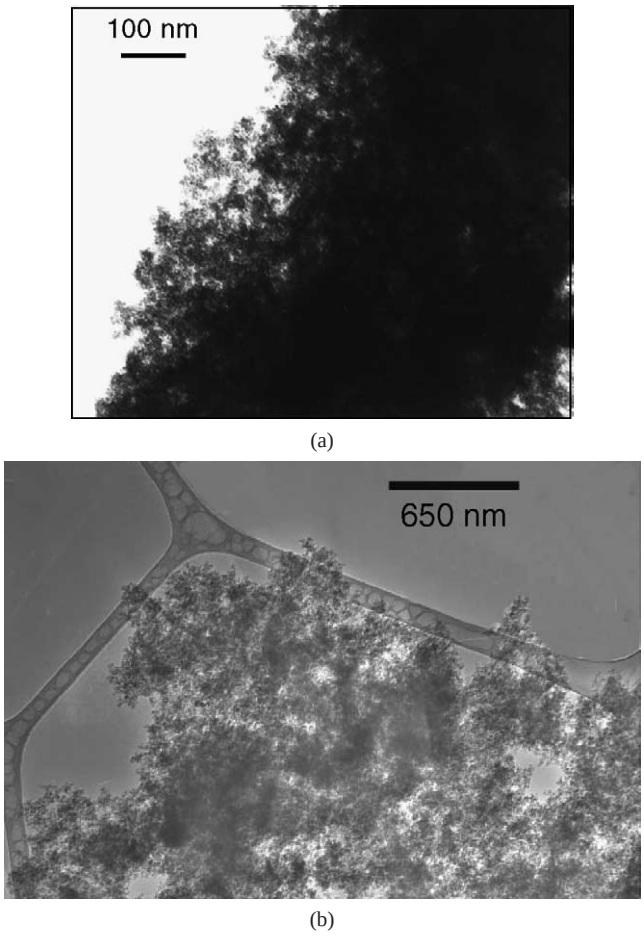

Fig. 5. TEM micrographs of $Ta_2O_5 \cdot 6SiO_2$ (a) and $Ta_2O_5 \cdot 18SiO_2$ (b).

metric stretching mode [43,49,50]. These observed bands at ca. 960 cm^{-1} are generally thought of as an overlap of two contributions (i.e., from the Ta–O–Si asymmetric stretching mode and the Si–OH mode). After calcination of these materials to 500 °C under flowing oxygen, the band for Ta–O–Si is still observed, suggesting that a high number of Ta–O–Si linkages remain intact.

Transmission electron microscopy (TEM) studies of $Ta_2O_5 \cdot 6SiO_2$ and $Ta_2O_5 \cdot 18SiO_2$ revealed aggregates of fine granules with a wide range of particle sizes, as shown in Fig. 5. Nitrogen porosimetry was used to further evaluate the pore structures and surface areas of the tantala–silica materials (Fig. 6). The adsorption–desorption data for both $Ta_2O_5 \cdot 6SiO_2$ and $Ta_2O_5 \cdot 18SiO_2$ correspond to type IV isotherms [51], suggesting some mesoporosity; however, a steep rise in adsorbed volume at relative pressure $(P/P_0) > 0.8$ is indicative of textural porosity [52]. The isotherm for $Ta_2O_5 \cdot 6SiO_2$ displays an H1 hysteresis (IUPAC classification) that is indicative of a porous material consisting of voids between agglomerates (i.e., rigidly joined particles) [51]. The isotherm for $Ta_2O_5 \cdot 18SiO_2$, on the other hand, displays an H3 hysteresis that is indicative of an almost nonporous material consisting of aggregates (i.e., loosely coherent particles) [51]. In both cases, the materials possess a wide range of pore sizes, with a considerable amount of micropores with radii smaller than 20 Å (Fig. 6). The materials were found to have relatively high BET surface areas [53], ranging from 450 $m^2\,g^{-1}$ for $Ta_2O_5 \cdot 6SiO_2$ to 200 $m^2\,g^{-1}$ for $Ta_2O_5 \cdot 18SiO_2$. It has similarly been observed that co-thermolysis of the $Zr[OSi(O^tBu)_3]_4$ molecular precursor with TEOS resulted in a surface area lower than that of the parent $ZrO_2 \cdot 4SiO_2$ material [27]. Calcination of $Ta_2O_5 \cdot 6SiO_2$ to 500 °C under oxygen did not result in a change in surface area (440 $m^2\,g^{-1}$), and likewise calcination of $Ta_2O_5 \cdot 18SiO_2$ to 500 °C resulted in essentially no change in surface area (220 $m^2\,g^{-1}$). Calcination of these

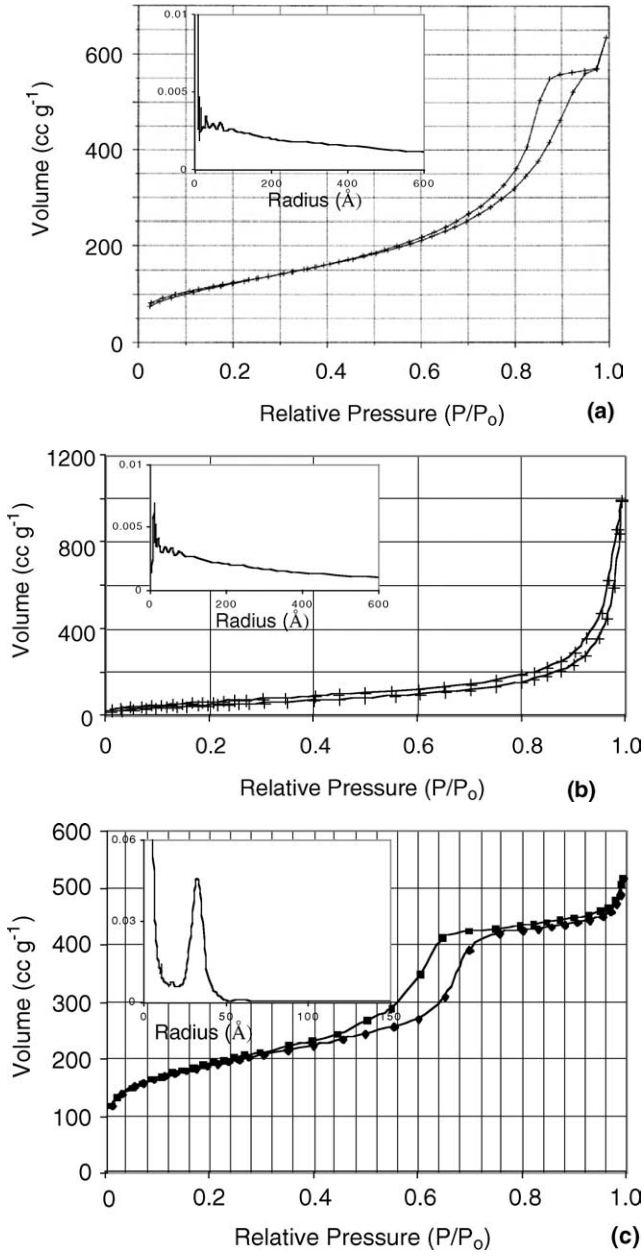

Fig. 6. Nitrogen adsorption–desorption isotherms for $Ta_2O_5 \cdot 6SiO_2$ (a) and $Ta_2O_5 \cdot 18SiO_2$ (b), and TaSBA-15 (c). Pore size distributions calculated from the adsorption isotherm branch are shown as insets.

materials to 1000 °C resulted in a substantial loss of surface area (to $< 5\ m^2\ g^{-1}$), however.

3.5. Synthesis and characterization of surface-supported TaSBA-15

In addition to the tantala–silica xerogels, a catalyst was prepared by grafting **1** onto a mesoporous SBA-15 substrate (SA = 690 $m^2\ g^{-1}$, OH coverage = 2.0 nm^{-2}). The grafting was accomplished via the addition of **1** (0.015 mmol) to the substrate (120 mg) to give a material with 1.51 wt% (Si/Ta = 200/1) tantalum loading, as determined by inductively coupled atomic emission spectroscopy (ICPAES). A subsequent catalyst was prepared by calcination of the TaSBA-15 material to 300 °C under oxygen to remove the organic moieties of the molecular precursor. This low weight loading should result in single-site tantalum centers on the silica surface [25,26]. Furthermore, the grafted materials have surface areas (310 $m^2\ g^{-1}$) that are reduced relative to that of the SBA-15 support; however, their ordered mesostructure was maintained, as evidenced by retention of the low-angle (100) reflection in the powder X-ray diffraction pattern. The adsorption–desorption data for TaSBA-15 correspond to a type IV isotherm, characteristic of mesoporous SBA-15 materials (Fig. 6c) [25]. The pore size distribution was observed to be relatively narrow, and the average pore radius, as determined by the nitrogen adsorption isotherm, was 33 Å. The pore structure of TaSBA-15 stands in contrast with that of the $Ta_2O_5 \cdot 6SiO_2$ and $Ta_2O_5 \cdot 18SiO_2$ xerogels, in that it has a well-defined, mesoporous, hexagonally ordered pore structure (by nitrogen porosimetry and low-angle X-ray diffraction).

Solution ^1H NMR spectroscopy was used to monitor the grafting chemistry of **1**. The reaction of surface Si–OH groups with **1** resulted in the elimination of 1.5 equiv of $(^tBuO)_3SiOH$ per grafted molecule of **1**. This suggests that the tantalum species bind to the silica surface via 1 or 2 Si–O–Ta linkages, and that the two structures are equally abundant

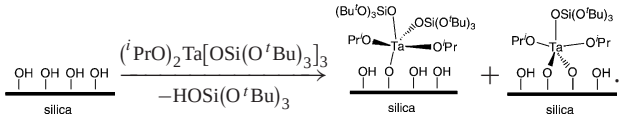

(2)

Also, based on the initial OH coverage of the support, the precursor reacts with only ca. 6% of the available OH sites with a 1.51 wt% Ta loading. The exact structure of the surface–bound Ta species is currently unknown, however, because of a lack of spectroscopic handles for such a low-abundance species. The observed band at ca. 960 cm^{-1} for the Ta–O–Si asymmetric stretching mode is not observed in the FTIR spectrum (Fig. 4), presumably as a result of the low Ta wt%. The M–O–Si stretching mode was also not observed in similarly prepared TiSBA-15 materials [25]. Furthermore, the ^{29}Si MAS NMR spectrum for TaSBA-15 reveals a broad resonance centered at −110 ppm that spans the chemical shift range for Q^2, Q^3, and Q^4 silicon environments (Fig. 3). The resonance for TaSBA-15 is further shifted toward the Q^4 chemical shift range as compared with the spectra for $Ta_2O_5 \cdot 6SiO_2$ and $Ta_2O_5 \cdot 18SiO_2$, suggesting a more fully condensed SiO_2 network.

3.6. Catalytic oxidation of cyclohexene

Samples of $Ta_2O_5 \cdot 6SiO_2$ and $Ta_2O_5 \cdot 18SiO_2$ (calcined to 500 °C) were found to exhibit catalytic activity for the oxidation of cyclohexene with TBHP, CHP, and aqueous H_2O_2 as the oxidants. The surface-supported TaSBA-15 catalyst was also found to be active for the oxidation of cyclohexene with TBHP, CHP, and aqueous H_2O_2.

To compare the activities for the heterogeneous catalysts (Table 1), we standardized the results with respect to mass of catalyst (0.035 g). In control experiments with catalyst and no oxidant, or with oxidant and no catalyst, no cyclohexene oxidation products were observed by GC analysis. In addition, catalysts were stirred in acetonitrile and cyclohexene for 1 h at 65 °C before addition of the oxidant. The solution was then hot-filtered after 10 min and stirred for 2 h at 65 °C. There was no significant oxidation of cyclohexene after the hot filtration, suggesting that leaching of catalytically active, soluble tantala species is negligible under these experimental conditions.

In Fig. 7, the results of cyclohexene oxidation with the use of several tantala–silica catalysts (on a per-gram basis) are depicted. The TaSBA-15 catalyst exhibited a higher activity for the oxidation of cyclohexene than the tantala–silica xerogels after 2 h. Use of TaSBA-15 as the catalyst (65 °C in acetonitrile) with H_2O_2 yielded 13.6% of oxidation products after 2 h (based on oxidant), whereas $Ta_2O_5 \cdot 6SiO_2$ and

Table 1
Tantalum-catalyzed oxidation of cyclohexene with H_2O_2 (65 °C, reaction time = 2 h)

Catalyst	Selectivity cyclohexene oxide (%)	Selectivity cyclohexenol (%)	Selectivity cyclohexenone (%)	Total yield based on H_2O_2 (%)	Initial rate[a] (mol oxidation products/(molTa(V) cat min))
$Ta_2O_5 \cdot 6SiO_2$	9.60	58.6	31.8	2.61	0.13
$Ta_2O_5 \cdot 18SiO_2$	17.2	37.9	44.9	4.70	0.22
TaSBA-15	36.0	32.7	31.3	13.6	6.70
TaSBA-15 (300 °C)	42.7	25.3	32.0	5.32	3.45

[a] Initial rate measured as the slope of the tangent to the plot of concentration versus time at $t = 0$, normalized per mol of Ta(V).

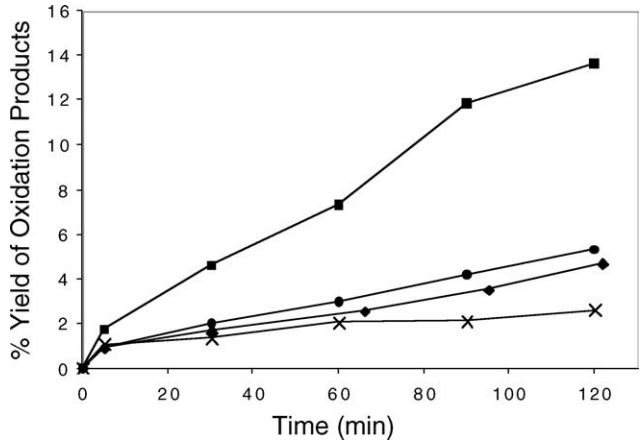

Fig. 7. Yield of cyclohexene oxidation products relative to initial H_2O_2 concentration as a function of time during the oxidation of cyclohexene with 0.035 g of TaSBA-15 (■), TaSBA-15 (300 °C) (●), $Ta_2O_5 \cdot 18SiO_2$ (◆), and $Ta_2O_5 \cdot 6SiO_2$ (×).

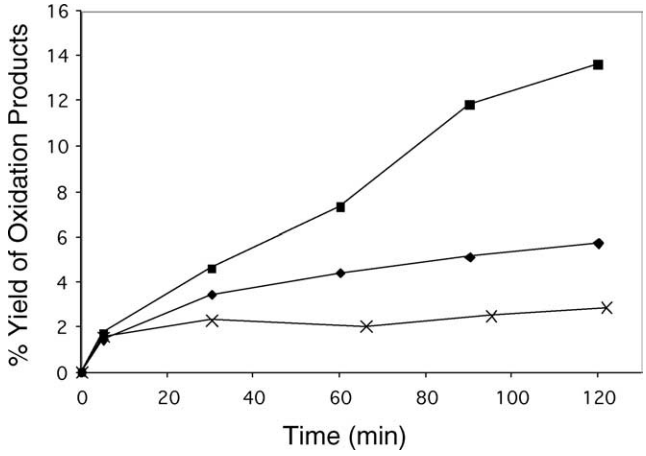

Fig. 8. Yield of cyclohexene oxidation products relative to initial H_2O_2 (■), CHP (◆), and TBHP (×) concentrations as a function of time during the oxidation of cyclohexene with 0.035 g of TaSBA-15.

$Ta_2O_5 \cdot 18SiO_2$ under analogous conditions yielded 2.6% and 4.7% of oxidation products, respectively. Calcination of the TaSBA-15 material to 300 °C under oxygen yielded a catalyst with lower activity (5.3% yield of cyclohexene oxidation as compared with 13.6%), which is consistent with previous results on titanium-based catalysts [25]. Calcination may result in migration of the tantalum into the framework silica, possibly facilitated by the siloxide ligands of **1** that would be converted to new surface silica centers. The TaSBA-15 catalysts are more selective for cyclohexene oxide formation (36–43%, 2 h), and $Ta_2O_5 \cdot 6SiO_2$ and $Ta_2O_5 \cdot 18SiO_2$ are less selective (10 and 17%, respectively). Over the course of 2 h, the selectivity for cyclohexene oxide drops as the abundance of allylic oxidation products increases (e.g., initial selectivity of 52% for cyclohexene oxide with the TaSBA-15 catalyst).

The results of cyclohexene oxidation with TaSBA-15 and three different oxidants (TBHP, CHP, and H_2O_2) are shown in Fig. 8. It appears that aqueous H_2O_2 is the most active

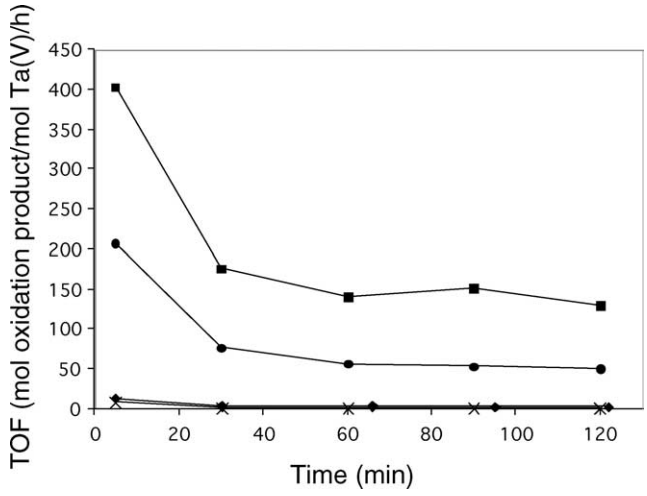

Fig. 9. Turnover frequencies (TOFs) as a function of time during the oxidation of cyclohexene with TaSBA-15 (■), TaSBA-15 (300 °C) (●), $Ta_2O_5 \cdot 18SiO_2$ (◆), and $Ta_2O_5 \cdot 6SiO_2$ (×). TOF = moles of cyclohexene oxidation products per mol Ta(V) per hour.

oxidant; the two organic peroxides have comparably lower activities. The selectivities achieved with the different oxidants are markedly different, however. Use of the organic peroxides results in high selectivities for cyclohexene oxide formation (94 and 70% with CHP and TBHP, respectively), whereas H_2O_2 is much less selective for epoxidation (36%).

Fig. 9 illustrates the catalyst activities in turnover frequencies (TOF), defined as the moles of oxidation product per mole Ta(V) per hour. The cyclohexene oxidation is generally more rapid (regardless of oxidant or catalyst) over the first 30 min of the reaction, and then the reaction slows for the remaining 90 min. This is attributed to increasing quantities of water or alcohol formation with time, thereby hindering formation of the tantalum-hydroperoxide complex by strong binding of polar species [54]. The initial rate of cyclohexene oxidation, as shown in Table 1, was greater with the TaSBA-15 catalysts (initial rate = 6.70 mol oxidation products/(mol Ta(V) cat min)). These results are possibly due to the presence of substrate-available, authentic surface tantalum sites in the mesopores of the TaSBA-15 catalyst. The xerogel catalysts, on the other hand, have considerable amounts of tantalum that are unavailable to substrate throughout the microporous bulk of the material and buried within in the silicate walls. It is well established that cyclohexene cannot be oxidized in a microporous TS1 material because of size constraints for the cyclohexene oxide product [55]. The pores of the TaSBA-15 catalyst should be large enough that diffusion does not limit the reaction rate with acetonitrile as the solvent. The xerogel catalysts, however, have a considerably microporous character and might be affected by diffusion limitations and steric constraints. Potential differences in observed rates caused by diffusion effects, particle size differences, hydrophobicity differences, etc. were not examined. Specific surface areas of the catalysts do not seem to affect the activity of these cat-

alysts, at least in the high-surface-area regime studied here ($> 200\ m^2\ g^{-1}$).

The catalyst activities reported here for the oxidation of cyclohexene are comparable to the activities recently reported for niobia–silica catalysts under similar conditions [55]. Hartmann and co-workers reported cyclohexene oxide yields of up to 15% (after 2 h) for microporous crystalline NbS-1 and Nb/silicalite-1 catalysts, with selectivities up to 80% for cyclohexene oxide formation. A mesoporous, noncrystalline NbMCM-41 catalyst provided good yields of cyclohexene oxidation products (ca. 20–45% after 2 h) as well [33,56]. In contrast, previously reported SBA-15-supported, single-site Ti(IV) catalysts are much more active (98% yield of oxidation products) for the oxidation of cyclohexene and give cyclohexene oxide selectively (90–100%) [25]. This Ti(IV) system was limited to the use of organic peroxides (CHP, TBHP), however, with yields less than 5% obtained when aqueous H_2O_2 was used. It appears that titanium cyclohexene oxidation catalysts are inherently more active, but comparable group V niobium and tantalum catalysts can operate when aqueous H_2O_2 is used as the oxidant.

4. Conclusions

Here we described the preparation and characterization of a new bis(alkoxy)tris(siloxy)tantalum(V) single-source molecular precursor, $(^{i}PrO)_2Ta[OSi(O^{t}Bu)_3]_3$ (**1**). This compound represents an interesting model for tantala sites in silica, and the single-crystal X-ray structure of an analogous compound, $(EtO)_2Ta[OSi(O^{t}Bu)_3]_3$ (**2**), provides structural information on such sites. The Ta–OSi bond distances of 1.860(5)–2.041(7) Å are similar to those previously reported by Roesky and co-workers for a model tantalum siloxide cage complex (1.984–1.987 Å) [47]. Both of these model complexes are in good agreement with Ta–OSi bond distances determined for silica-supported tantalum oxide by EXAFS analyses [42,50]. Furthermore, the ^{29}Si NMR chemical shift for **1** at −97.57 ppm provides an important spectroscopic reference for $Ta(V)/SiO_2$ systems. Because of a lack of analogous $TaOSiO_3$ model complexes, no direct spectroscopic ^{29}Si NMR comparisons can be made; however, a series of early transition-metal siloxy complexes of the type $MOSiO_3$ (M = Ti, Zr, Hf, V) has been prepared [41,57,58]. The group IV complexes of the type $M[OSi(O^{t}Bu)_3]_4$ exhibit ^{29}Si NMR resonances at −103.24, −100.50, and −97.06 ppm for M = Ti, Zr, and Hf, respectively. Moreover, a V(V)=O complex of the type $OV[OSi(O^{t}Bu)_3]_3$ exhibited a ^{29}Si NMR resonance at −98.00 ppm. The observed chemical shift for **1** comes where expected, compared with these slightly different early transition-metal siloxy complexes.

In this study it was shown that **1** is a versatile reagent for both the preparation of bulk tantala–silica xerogels and the grafting of tantalum centers onto the surface of silica. In addition, more silica-rich materials can be obtained through a co-thermolytic route with **1** and $HOSi(O^{t}Bu)_3$. This expands the tunability of the thermolytic molecular precursor route by allowing variable metal-to-silicon ratios. Furthermore, because $HOSi(O^{t}Bu)_3$ cleanly converts to SiO_2 via the stoichiometric elimination of isobutylene and water in the presence of tantalum, the presence of incompletely condensed alkoxy groups is avoided, unlike the case with TEOS [27].

To our knowledge, this work represents the first utilization of tantala–silica materials as cyclohexene oxidation catalysts. The most active catalyst for the oxidation of cyclohexene has grafted tantala sites (TaSBA-15) and uses H_2O_2 as the oxidant in acetonitrile at 65 °C (initial rate of 6.70 mole oxidation product per mole Ta(V) per minute). The organic peroxides TBHP and CHP are also viable and more selective, but less active, oxidants. Conversely, previously reported TiSBA-15 catalysts were extremely active in cyclohexene epoxidation with CHP and TBHP as oxidants but essentially inactive in combination with H_2O_2. This suggests that Ta(V) is more tolerant of the presence of water for cyclohexene oxidant than the analogous Ti(IV) system, which perhaps is a result of an extra coordination site for group V metals, assuming an equal number of surface Si–O–M linkages. It is interesting to note that Basset and co-workers have developed $Ta(V)/SiO_2$ catalysts that are very active in the epoxidation of allylic alcohols [29,30]. Given the observed activity of catalysts described here, this suggests that the activity of alkene oxidation by heterogeneous tantala–silica catalysts is highly substrate dependent.

Acknowledgment

This work was supported by the Director, Office of Energy Research, Office of Basic Energy Sciences, Chemical Sciences Division, of the US Department of Energy under Contract DE-AC03-76SF00098. R.L.B. thanks the National Science Foundation for support with a NSF Graduate Fellowship. We thank P. Yu at the University of California, Davis, for the MAS NMR spectra and A.M. Stacy at the University of California, Berkeley, for the use of instrumentation (PXRD). We are grateful to A. Tolley for technical assistance with electron microscopy and the National Center for Electron Microscopy for the use of their microscopes.

Supplementary material

Experimental and characterization data and selected bond angles and distances for **2**.

Please visit DOI: 10.1016/j.jcat.2004.10.015.

References

[1] D.R. Uhlmann, D.R. Ulrich (Eds.), Ultrastructure Processing of Advanced Materials, Wiley–Interscience, New York, 1992.

[2] A.K. Cheetham, C.J. Brinker, M.L. Mecartney, C. Sanchez (Eds.), Better Ceramics Through Chemistry VI, in: Materials Research Society Symposium Proceedings, vol. 360, Materials Research Society, Pittsburgh, 1994, and previous volumes.
[3] C.L. Bowes, G.A. Ozin, Adv. Mater. 8 (1996) 13.
[4] C.J. Brinker, G.W. Scherer, Sol–Gel Science, Academic Press, Boston, 1990.
[5] C.J. Brinker, J. Non-Cryst. Solids 100 (1988) 31.
[6] R.J.P. Corriu, D. Leclercq, Agnew. Chem., Int. Ed. Engl. 35 (1996) 1421.
[7] B. Wang, A.B. Brennan, H. Huang, G.L. Wilkes, J. Macromol. Sci., Chem. A27 (1990) 1447.
[8] B. Wang, G.L. Wilkes, C.D. Smith, J.E. McGrath, Polym. Commun. 32 (1991) 400.
[9] B. Wang, G.L. Wilkes, J. Polym. Sci., Part A: Polym. Chem. 29 (1991) 905.
[10] B. Wang, G.L. Wilkes, J.C. Hedrick, S.C. Liptak, J.E. McGrath, Macromolecules 24 (1991) 3449.
[11] G. Kickelbick, U. Schubert, J. Chem. Soc., Dalton Trans. (1997) 1301.
[12] L.-H. Lee, W.-C. Chen, Chem. Mater. 13 (2001) 1137.
[13] U. Schubert, T. Völkel, N. Moszner, Chem. Mater. 13 (2001) 3811.
[14] A.H. Cowley, R.A. Jones, Agnew. Chem., Int. Ed. Engl. 28 (1989) 1208.
[15] A.W. Apblett, A.C. Warren, A.R. Barron, Chem. Mater. 4 (1992) 167.
[16] F. Chaput, A. Lecomte, A. Dauger, J.P. Boilot, Chem. Mater. 1 (1989) 199.
[17] L.G. Hubert-Pfalzgraf, New J. Chem. 11 (1987) 663.
[18] R.C. Mehrotra, J. Non-Cryst. Solids 121 (1990) 1.
[19] D.C. Bradley, Polyhedron 13 (1994) 1111.
[20] C.D. Chandler, C. Roger, M.J. Hampden-Smith, Chem. Rev. 93 (1993) 1205.
[21] C.K. Narula, A. Varshney, U. Riaz, Chem. Vap. Deposition 2 (1996) 13.
[22] A. Altherr, H. Wolfganger, M. Veith, Chem. Vap. Deposition 5 (1999) 87.
[23] T.D. Tilley, J. Mol. Catal. 182–183 (2002) 17.
[24] K.L. Fujdala, T.D. Tilley, J. Catal. 216 (2003) 265.
[25] J. Jarupatrakorn, T.D. Tilley, J. Am. Chem. Soc. 124 (2002) 8380.
[26] C. Nozaki, C.G. Lugmair, A.T. Bell, T.D. Tilley, J. Am. Chem. Soc. 124 (2002) 13194.
[27] R.L. Brutchey, J.E. Goldberger, T.S. Koffas, T.D. Tilley, Chem. Mater. 15 (2003) 1040.
[28] R.J. Saxton, J.G. Zajacek, US Patent 5,618,512 (1992).
[29] D. Meunier, A. Piechaczyk, A. de Mallmann, J.M. Basset, Agnew. Chem., Int. Ed. Engl. 38 (1999) 3540.
[30] D. Meunier, A. de Mallmann, J.M. Basset, Top. Catal. 23 (2003) 183.
[31] M. Ziolek, I. Nowak, I. Sobczak, A. Lewandowska, P. Decyk, J. Kujawa, Stud. Surf. Sci. Catal. 129 (2000) 813.
[32] J. Xin, J. Suo, X. Zhang, Z. Zhang, New J. Chem. 24 (2000) 813.
[33] I. Nowak, B. Kilos, M. Ziolek, A. Lewandowska, Catal. Today 78 (2003) 487.
[34] V. Parvulescu, C. Constatin, B.L. Su, J. Molec. Catal. 202 (2003) 171.
[35] T. Ushikubo, Catal. Today 57 (2000) 331.
[36] D.C. Bradley, B.N. Chakravarti, A.K. Chatterjee, W. Wardlaw, A. Whitley, J. Chem. Soc. (1958) 99.
[37] Y. Abe, I. Kijima, Bull. Chem. Soc. Jpn. 42 (1969) 1118.
[38] D. Zhao, Q. Huo, J. Feng, B.F. Chmelka, G.D. Stucky, J. Am. Chem. Soc. 120 (1998) 6024.
[39] P.T. Wolczanski, Polyhedron 14 (1995) 3335.
[40] D.C. Bradley, I.M. Thomas, J. Chem. Soc. (1959) 3404.
[41] K.W. Terry, C.G. Lugmair, T.D. Tilley, J. Am. Chem. Soc. 119 (1997) 9745.
[42] T. Tanaka, H. Nojima, T. Yamamoto, S. Takenaka, T. Funabiki, S. Yoshida, Phys. Chem. Chem. Phys. 1 (1999) 5235.
[43] G. Guiu, P. Grange, Bull. Chem. Soc. Jpn. 67 (1994) 2716.
[44] International Center for Diffraction Data “PC-PDF”, vol. 2, 1988, Card# 25-922.
[45] S.M. Maurer, E.I. Ko, Catal. Lett. 72 (1992) 231.
[46] M.I. Osendi, J.J. Moya, C.J. Serna, J. Soria, J. Am. Ceram. Soc. 68 (1985) 135.
[47] A.I. Gouzyr, H. Wessel, C.E. Barnes, H.W. Roesky, M. Teichert, I. Usón, Inorg. Chem. 36 (1997) 3392.
[48] Z. Fei, S. Busse, F.T. Edelmann, J. Chem. Soc., Dalton Trans. (2002) 2587.
[49] M. Baltes, A. Kytökivi, B.M. Weckhuysen, R.A. Schoonheydt, P. van der Voort, E.F. Vansant, J. Phys. Chem. B 105 (2001) 6211.
[50] D.M. Pickup, G. Mountjoy, M.A. Holland, G.W. Wallidge, R.J. Newport, M.E. Smith, J. Mater. Chem. 10 (2000) 1887.
[51] K.S.W. Sing, Pure Appl. Chem. 57 (1985) 603.
[52] P.T. Tanev, T.J. Pinnavaia, Chem. Mater. 8 (1996) 2068.
[53] S.J. Gregg, K.S.W. Sing, Adsorption, Surface Area, and Porosity, second ed., Academic Press, London, 1982.
[54] R.A. Sheldon, J. Molec. Catal. 7 (1980) 107.
[55] M. Hartmann, A.M. Prakash, L. Kevan, Catal. Today 78 (2003) 467.
[56] B. Kilos, M. Aouine, I. Nowak, M. Ziolek, J.C. Volta, J. Catal. 224 (2004) 314.
[57] M.P. Coles, C.G. Lugmair, K.W. Terry, T.D. Tilley, Chem. Mater. 12 (2000) 122.
[58] R. Rulkens, J.L. Male, K.W. Terry, B. Olthof, A. Khodakov, A.T. Bell, E. Iglesia, T.D. Tilley, Chem. Mater. 11 (1999) 2966.